2014

Infrared vibrational and electronic transitions in the dibenzopolyacene family

Andrew Mattioda
NASA Ames Research Center, Andrew.Mattioda@nasa.gov

Charles Baushlicher Jr.
Carl Sagan Center, SETI Institute

Jonathan Bregman
NASA Ames Research Center

Douglas Hudgins
NASA Ames Research Center

Louis Allamandola
NASA Ames Research Center

See next page for additional authors

Spectrochimica Acta Part A: Molecular and Biomolecular Spectroscopy 130 (2014) 639–652

Contents lists available at ScienceDirect

Spectrochimica Acta Part A: Molecular and Biomolecular Spectroscopy

journal homepage: www.elsevier.com/locate/saa

Infrared vibrational and electronic transitions in the dibenzopolyacene family

Andrew L. Mattioda [a,*,1], Charles W. Bauschlicher Jr. [a,*,2], Jonathan D. Bregman [a,1], Douglas M. Hudgins [a,1,3], Louis J. Allamandola [a,1], Alessandra Ricca [b]

[a] NASA Ames Research Center, Moffett Field, CA 94035, United States
[b] Carl Sagan Center, SETI Institute, 189 Bernardo Ave., Suite 100, Mountain View, CA 94043, United States

HIGHLIGHTS

- Experimental spectra in the mid- and near-IR and DFT calculations for the vibrational and electronic spectra are reported.
- Good agreement between theory and experiment for the vibrational frequencies of the neutral species.
- The intensity of the 1440 cm^{-1} band grows with molecular size.
- B3LYP fails for ions, BP86 is in reasonable agreement with experiment.
- The large molecules show electronic transitions in the mid-IR and theory gives insight into these transitions.

GRAPHICAL ABSTRACT

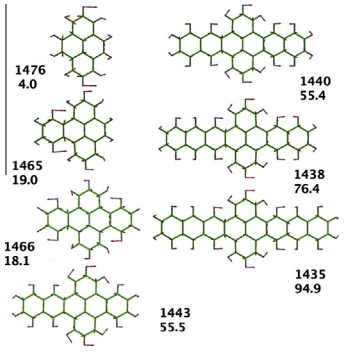

ARTICLE INFO

Article history:
Received 30 January 2014
Received in revised form 2 April 2014
Accepted 3 April 2014
Available online 18 April 2014

Keywords:
Matrix isolation
DFT
Infrared spectroscopy
Vibrational spectroscopy
Electronic transitions
Polycyclic aromatic hydrocarbons

ABSTRACT

We report experimental spectra in the mid-infrared (IR) and near-IR for a series of dibenzoacenes isolated in Ar matrices. The experiments are supported by Density Functional Theory (DFT) and Time-Dependent DFT (TD-DFT) calculations with both vibrational and electronic transitions studied. For the neutrals, we find good agreement between the experimental and B3LYP and BP86 results for all species studied. The band at about 1440 cm^{-1} carries more intensity than in typical PAHs and increases in intensity with the size of the dibenzoacene molecule. For the ions the B3LYP approach fails to yield reasonable IR spectra for most systems and the BP86 approach is used. Electronic transitions dominate the vibrational bands in the mid-IR region for the large dibenzoacene ions. In spite of the very strong electronic transitions, there is still reasonable agreement between theory and experiment for the vibrational band positions. The experimental and theoretical results for the dibenzoacenes are also compared with those for the polyacenes.

Published by Elsevier B.V.

Introduction

Over the past several years Polycyclic Aromatic Hydrocarbons, better known as PAHs, have witnessed a resurgence in research interest due to their applicability to diverse fields such as environmental science [1,2], health science [2,3], materials science [4–6] and astrophysics [7,8]. As a by-product of combustion, PAHs

* Corresponding authors. Tel.: +1 650 604 6231.
E-mail addresses: Andrew.Mattioda@nasa.gov (A.L. Mattioda), Charles.W.Bauschlicher@nasa.gov (C.W. Bauschlicher Jr.), Alessandra.Ricca-1@nasa.gov (A. Ricca).
[1] Space Science Branch, Mail Stop 245-6.
[2] Entry Systems and Technology Division, Mail Stop 230-3.
[3] Current address: NASA HQ, Washington, DC 20546, United States.

http://dx.doi.org/10.1016/j.saa.2014.04.017
1386-1425/Published by Elsevier B.V.

represent an environmental contaminant at many hazardous waste sites [1]. PAHs' carcinogenic properties make them of interest to health sciences [3]. Their aromatic and extended structures can potentially serve as building blocks to carbonaceous compounds ranging from carbon nanotubes to graphene, thus they are of considerable use in materials science [5]. Astronomical observations have shown that most interstellar and circumstellar objects in the Galaxy and many extra-galactic objects are emitting an infrared spectrum that is dominated by a family of highly vibrationally excited PAHs [7]. Thus PAHs are also of great interest to the astrophysical community.

One subset of the PAH family consists of the polyacene molecules (see Fig. 1, molecules I to O) composed of linearly annulated benzene subunits. The polyacenes unique structure has fascinated organic chemists for over a century [6,9–11], while their unique electronic structure has generated considerable interest from materials scientists, resulting in numerous investigations [11,12]. The π systems in the polyacene molecules have smaller highest occupied molecular orbital-lowest unoccupied molecular orbital (HOMO–LUMO) gaps than typically observed for similar-sized PAHs, with the energy gap decreasing with increasing polyacene length [13]. The changing electronic structure with increasing polyacene length eventually causes the polyacenes to shift from being insulators to p-type semiconductors. Unfortunately this also causes the polyacenes to become chemically reactive as well, with hexacene (composed of 6 benzene rings) slowly decomposing at room temperature. Although Clar reported [14] the synthesis of hexacene in 1942, its existence remained controversial until 2006, when its synthesis was finally reproduced in stabilizing matrices [13,15]. In 2009, the polyacene series from pentacene through heptacene was produced and investigated in a matrix-isolation study by Mondal et al. [13] In 2010 Tönshoff and Bettinger [16] reported the production, ultraviolet (UV) and infrared (IR) spectroscopic characterization of octacene and nonacene in an argon matrix.

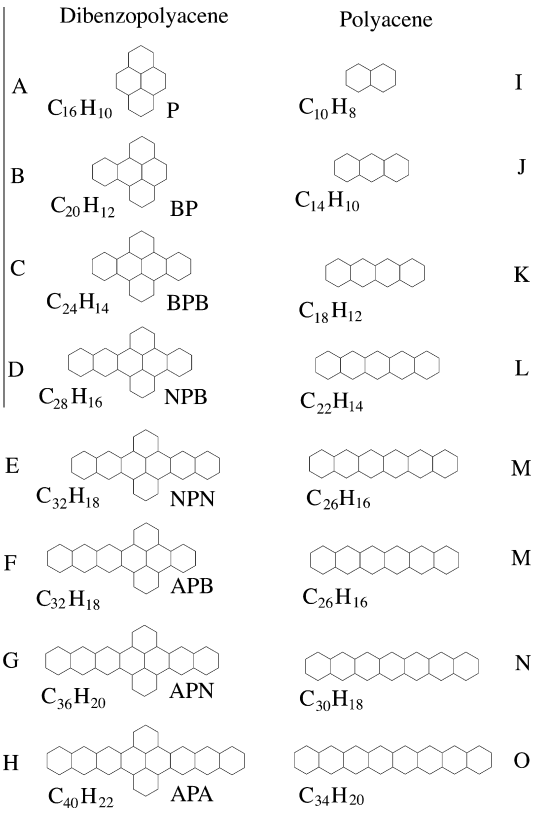

Fig. 1. Dibenzopolyacenes studied in this work and their polyacene analogs. The dibenzopolyacenes are denoted P through APA using the shorthand notation explained in Section 'Methods'.

Though the polyacene molecules are reactive, their derivatives seem to be more stable [17–19]. Payne et al. [17], Chun et al. [18], and Kaur et al. [19] have reported the synthesis of heptacene derivatives. Weisman et al. [20] have reported a theoretical and spectroscopic study of dibenzopolyacene molecules up to the dibenzo[jk,a1b1]octacene range. In their matrix-isolated study, Weisman et al. reported the remarkable finding of the presence of strong electronic transitions in the mid-IR for the radical cation and anions of dibenzo[jk,a1b1]octacene and dibenzo[hi,uv]hexacene.

The current work presents a mid-IR spectroscopic study of the neutral molecules from pyrene (dibenzonaphthlene) through dibenzo[jk,a1b1]octacene and a mid-IR and near IR (NIR) spectroscopic study of the radical cation and anions for dibenzo[fg,op]tetracene through dibenzo[jk,a1b1]octacene. This expands on the Weisman et al. study in several ways: first, we report the results for some less symmetric dibenzopolyacene molecules; second, we analyze the experiments in more detail to extract IR vibrational band positions and intensities; and third, we compare theory and experiment for the allowed IR vibrational transitions. The inclusion of the less symmetric species allows an understanding of the effect of both size and shape on the results. Finally, we note that we compute the electronic transitions using a different basis set and functional than used by Weisman et al. This allows an evaluation of the effect of basis set and functional on the results.

Methods

The dibenzopolyacene molecules studied here are shown in the left-hand column of Fig. 1. Their polyacene counterparts are shown in the right-hand column. All of the dibenzopolyacene molecules can be described as containing a pyrene core with side groups added to one or two sides. The side groups are benzo, naphtho, or anthro. Because the names are quite long, we use an XPY abbreviation, where the P denotes the pyrene central unit and the X and Y are the wings, of which B denotes benzo, N denotes naphtho and A denotes anthro.

Experimental techniques

The matrix-isolation mid-IR and NIR spectroscopic techniques employed in these studies have been described in detail elsewhere [20–24] and are briefly summarized here. Matrix isolated dibenzopolyacene samples were prepared by vapor co-deposition of the species of interest with an over abundance of argon (Ar) onto a 14 K CsI window suspended in a high-vacuum chamber ($p < 10^{-7}$ Torr). The deposition conditions produced an Ar/polyacene ratio in excess of 1000:1. After accumulation of a sufficient amount of neutral material, an IR spectrum of the sample was recorded.

Once the neutral spectra were recorded, cation and anion molecular species were generated *in situ* via vacuum UV photolysis of the PAH/Ar matrix. Photolysis was accomplished with the combined 120 nm Lyman α/160 nm very broad molecular hydrogen emission bands (10.1 and 7.77 eV, respectively) from a microwave-powered flowing H_2 discharge lamp with a dynamic pressure of 150 mTorr. An upper limit to the ionization efficiency can be obtained by measuring the percent decrease in the neutral band integrated areas that accompany photolysis, assuming that all neutral PAH molecules that disappear are converted into ions. For the pure Argon matrix experiments, ionization results in the formation of both cation and anion species. For the determination of the molecular absorbance (A values), we assume that one cation and

one anion are produced for every two neutral PAHs lost. Subtracting the unphotolyzed (neutral) spectrum from the photolyzed provides the ion spectrum. A second matrix isolation experiment, using an Ar/NO_2 matrix gas, is conducted. The presence of NO_2, an electron acceptor, in the matrix (at a concentration of approximately 1 part in 1000 in a typical experiment) ensures that the newly formed PAH bands all originate from the cation. By subtracting the Ar/NO_2 spectrum from the Ar ion spectrum, the anion bands are revealed. In a typical experiment, approximately 10–20% of the PAH molecules are ionized upon photolysis. NIR spectra of the matrix isolated radical anion and cation form of the XPY species were measured and compared with the analogous polyacenes. The deposition temperatures were: BPB 125 °C, NPB 195 °C, NPN 255 °C, APN 305 °C, and APA 365 °C.

Experimental samples (⩾99% purity) were obtained from the Institute for PAH Research, Greifenberg, Germany. Each spectrum was recorded on a Bio-Rad/Digilab Excalibur FTS-4000 IR spectrometer as a co-addition of 500 scans at a resolution of 0.5 cm^{-1}. For presentation purposes, the reported spectra have been baseline corrected. In some instances, several bands resulting from impurities (such as water, NO_2 and accompanying photoproducts) have been subtracted out or truncated using the Win-IR Pro 3.4 Software package. All numerical values cited in this paper are based on the band integrations of unaltered data.

The Win-IR Pro 3.4 (DigiLab) software package was used to determine the integrated intensities ($\int \tau d\nu$) for the observed bands. Absolute intensities ($A = (1/N)/\int \tau d\nu$), where N is the column density of absorbers (in molecules/cm^2) for the experimentally measured neutral PAHs were determined using the theoretical values as follows. The integrated intensities for all bands between 1500 and 500 cm^{-1} (6.67 and 20.0 μm, respectively) were summed to obtain the total absorption intensity over this region. This range was chosen to exclude the contributions of the far-IR bands (ν < 500 cm^{-1}) that were not measured in the experiments and the upper cutoff of ν > 1500 cm^{-1} excludes the CH stretching bands, which are substantially overestimated by quantum calculations [28], the overtone/combination bands that are present in the experimental data and not included in the theory, and interference from the water band contamination that fall in the 1625–1590 cm^{-1} range. These areas were put on an absolute footing using theoretically calculated absolute band intensities as described by Hudgins and Sandford [24]. Namely, the experimental relative intensities are scaled by the ratio of the sum of the theoretically computed intensities between 1500 and 500 cm^{-1} over the sum of the experimental intensities over the same range.

$$A_i^{exp} = I_{rel,i}^{exp} \frac{\sum_{\nu=500}^{1500} A^{thy}}{\sum_{\nu=500}^{1500} I_{rel}^{exp}} \quad (1)$$

This method takes advantage of the fact that although there may be some band-to-band variability in the accuracy of the calculated intensity, the total intensity is generally accurate to within 10–20%, excluding the CH stretching region.

For the electronic transitions, we report oscillator strengths (f values) that were determined as described by Kjaergaard et al. [25], namely we multiply the total integrated absorbance by 1.87×10^{-7} mol/km.

Theoretical techniques

Our PAH database [8], which is available at www.astrochem.org/pahdb, contains more than 600 PAH species, which includes PAH molecules with up to 384 carbon atoms. This data is being used to model observed astronomical spectra and therefore it is important that all species be treated with as similar an approach as possible. Because PAH molecules containing up to about 150 carbon atoms are believed to exist in the interstellar medium [26], the database must contain many large molecules. This requires the use of a small basis set, such as 4-31G [27]. Luckily calibration studies [28] have shown that, in most cases, reliable frequencies and IR intensities can be obtained using the hybrid [29] B3LYP [30] approach in conjunction with the 4-31G basis set. Since we will add the molecules studied in this work to the database, we use the same level of theory as in previous work. We should note that for some systems in this work we use larger basis sets when problems arise in the calculation of the vibrational frequencies. In addition, a larger basis set is used to calibrate the electronic excitations, where far less experience using the 4-31G basis set exists.

The structures have been fully optimized and the harmonic frequencies computed using density functional theory (DFT). We have used the hybrid B3LYP functional and the generalized gradient approximation (GGA) Becke-Perdew86 [31,32] (BP86) functional. The 4-31G basis set [27] has been used in all calculations unless otherwise noted.

Previous work [28] has shown that the hybrid B3LYP functional usually yields reliable vibrational frequencies and is therefore our functional of choice. However, like all functionals, it can fail to yield reliable results in some cases. In addition to rare, but easy to detect, catastrophic failures, there is a much more common failure where some of the intensities are too large. This problem is not due to spin contamination, but rather to a mixing of higher lying states during the calculation of the vibrational frequencies [33]. For PAHs, this intensity problem can be detected by comparing PAH spectra, because molecules of similar size and with the same charge have approximately the same total intensity. This type of failure is more common for hybrid functionals than for GGA functionals [33,34]. In those cases where the B3LYP functional appears to be unreliable, we have used the BP86 approach to test the B3LYP approach, since previous work [34,35] has shown that BP86 commonly works in those cases where B3LYP fails. In this work we have found that all of the ions, except pyrene$^+$ and benzopyrene$^+$, must be treated with the BP86 approach. NPB$^+$ is an exception, where both B3LYP and BP86 break symmetry and fail to yield a reliable IR spectra. This happens when there is a very low-lying state for both functionals, which is less common than having a very low-lying state for only the hybrid functional. NPB$^-$ is another ion where problems arise. While it has the expected symmetry, its IR spectrum is inconsistent with that of other PAH molecules at both the B3LYP and BP86 levels. However, we found that expanding the basis set to 6-31+G(d) yields a BP86 IR spectrum that is consistent with that of other PAH anions. Thus both choice of functional and basis set have an influence on the subtle failure mechanism.

Previous work [28] has shown that the computed B3LYP/4-31G harmonic frequencies scaled by a single scale factor of 0.958 are in excellent agreement with the matrix isolation Mid-IR fundamental frequencies of PAH molecules. This approach has been confirmed [36] in subsequent studies for molecules with sizes up to $C_{48}H_{20}$. For the BP86 calculations the scale factor is 0.986 for the 4-31G basis set. Two scale factors are used for the NPB$^-$ calculations using the 6-31+G(d) basis set, namely 1.003 for the C–H stretch and 0.9858 for all other modes. These scale factors were deduced using naphthalene experimental data following our previously published [34] procedure.

The electronic excitations have been determined using time-dependent density functional theory (TD-DFT). We report on calibration calculations on NPN where the choice of basis set, geometry, and functional are considered. On the basis of these calibration calculations and the fact that experience has shown that hybrid functionals yield better excitation energies than GGA functionals, we use the B3LYP/4-31G//B3LYP/4-31G level for all TD-DFT calculations.

All calculations have been performed using Gaussian 09 [37] or earlier versions of the same program system. The interactive molecular graphics tool MOLEKEL [38] has been used to aid the analysis of the vibrational modes.

Results and discussions

Neutral molecules Mid-IR

The complete results for the molecules studied in this work can be found in our database at www.astrochem.org/pahdb after publication. For BPB, NPB, NPN, APN, and APA experimental and computational vibrational band positions and intensities are reported, whereas for APB, only computational results are available. We also include results for the previously published [39] P and BP for comparison. The molecules larger than BPB are nonplanar, with the polyacene unit bending up and the pyrene part bending down. The results of the infrared spectroscopic investigation are summarized in Figs. 2–5. A detailed comparison of the experimental and theoretical results is given in supplemental Tables S1–S5. The obvious experimental combination and overtone bands with frequencies higher than 1600 cm^{-1} are not reported as they are missing from theory, which uses the harmonic approximation. For publication purposes, if both the experimental and theoretical intensities are less than 2 km/mol in intensity, they are not reported in the Tables S1–S5. Note that the sum of the intensities

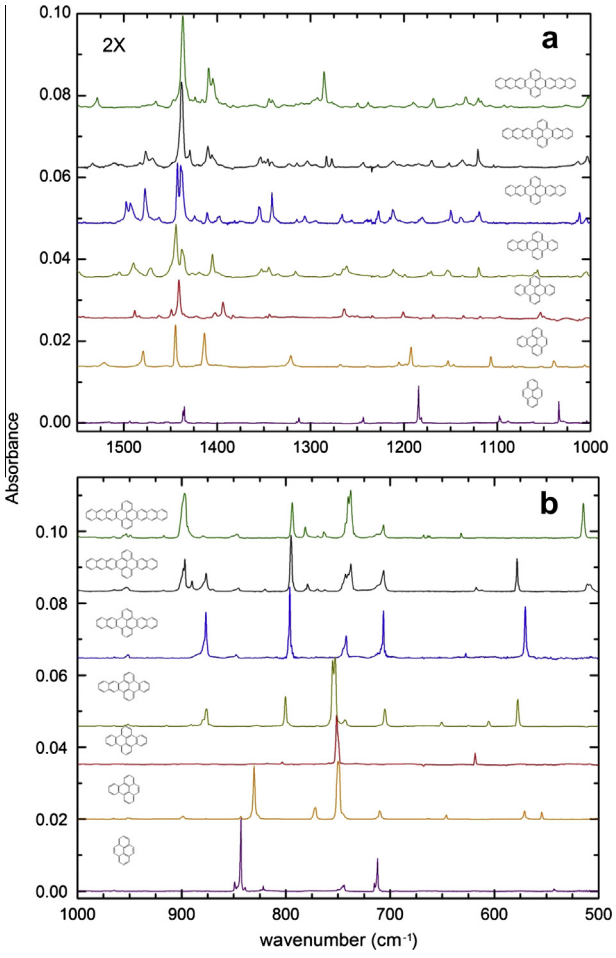

Fig. 2. Matrix-Isolated infrared spectra of: (a) C–H and C–C in-plane motions and (b) C–H out-of-plane motions for the neutral dibenzopolyacene family: P, BP, BPB, NPB, NPN, APN, and APA.

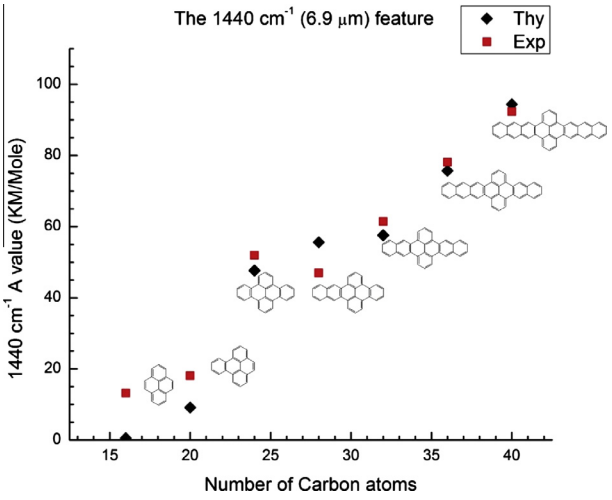

Fig. 3. Comparison of the intensity (experimental and theoretical) of the 1440 cm^{-1} feature in the dibenzopolyacenes with increasing polyacene length.

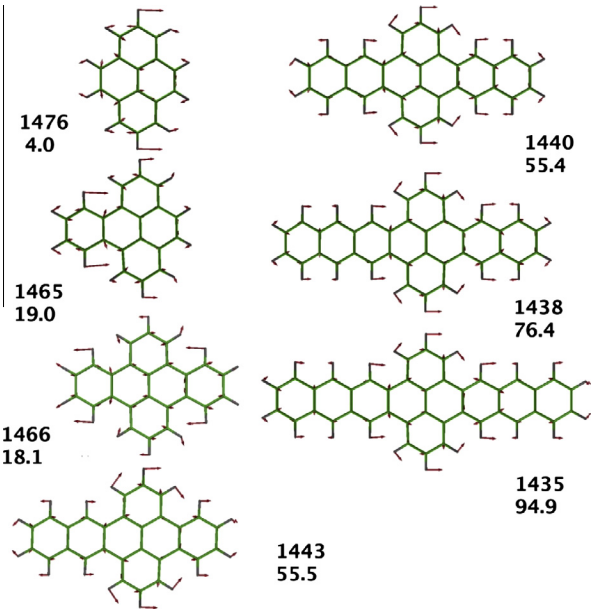

Fig. 4. The vibrational motion associated with the 1440 cm^{-1} band is shown. For each molecule we give the band position, in cm^{-1}, and its intensity, in km/mol.

from 500 to 1500 cm^{-1} reported in the tables included all bands, not just those reported in the tables. While we believe that the B3LYP results are superior to the BP86 results for the neutrals, we report the BP86 results as well to allow a comparison of the two functionals since the BP86 approach was used for most of the ions. Both the band position and the intensity were used to match the theory and experiment to each other. Forbidden bands (denoted as FB) were only used when there were no allowed bands available, and these assignments must be considered tentative at best.

An inspection of the Tables S1–S5 shows that there is excellent agreement between the theoretical calculations and the experimental values, with a few exceptions. In several instances the BP86 and/or B3LYP theoretical results exhibit bands greater than 2 km/mol in intensity that have no corresponding mode in the experimental spectra. However, these modes are typically less than 6 km/mol in intensity and may be obscured in the experimental results or be a computational artifact arising from mixing of modes

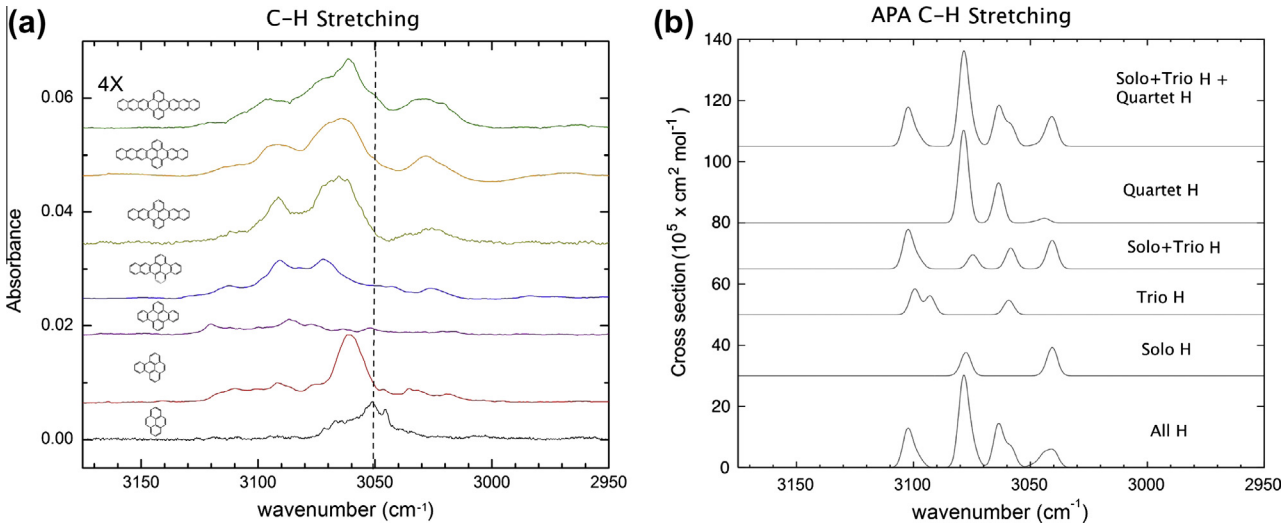

Fig. 5. (a) Matrix-Isolated infrared spectra of C–H stretching motions for the neutral dibenzopolyacene family: P, BP, BPB, NPB, NPN, APN, and APA. (b) Calculated C–H stretching region for APA. The H atoms that are not deuteriums are given. For example "Solo H" means the solo H atoms are hydrogens while the remaining H atoms are deuteriums.

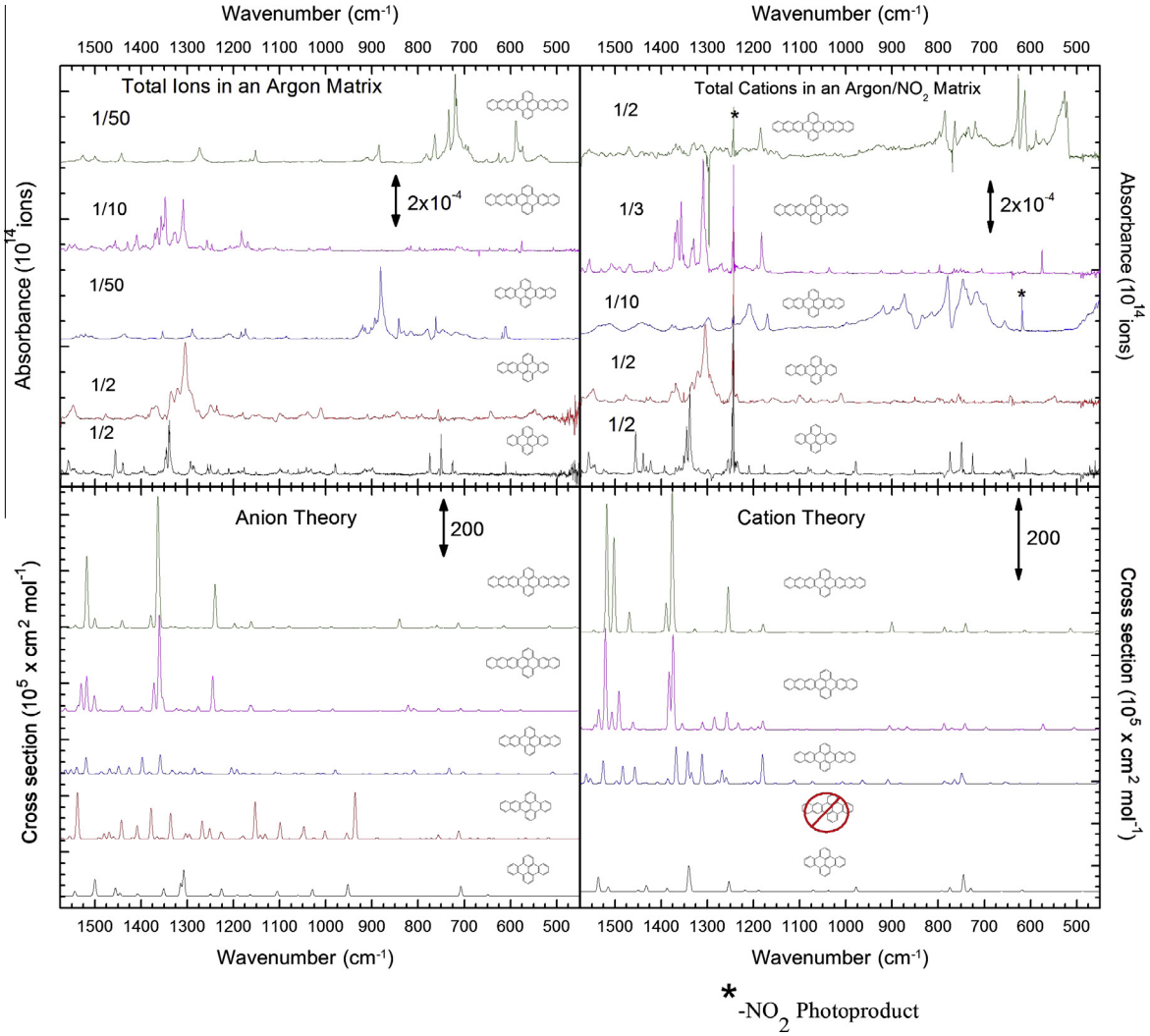

Fig. 6. Experimental mid-IR (top) and theoretical (bottom) vibrational spectra for the anions and cations. The Ar matrix spectra contains both cations and anions, while the Ar/NO_2 spectra should have only cations.

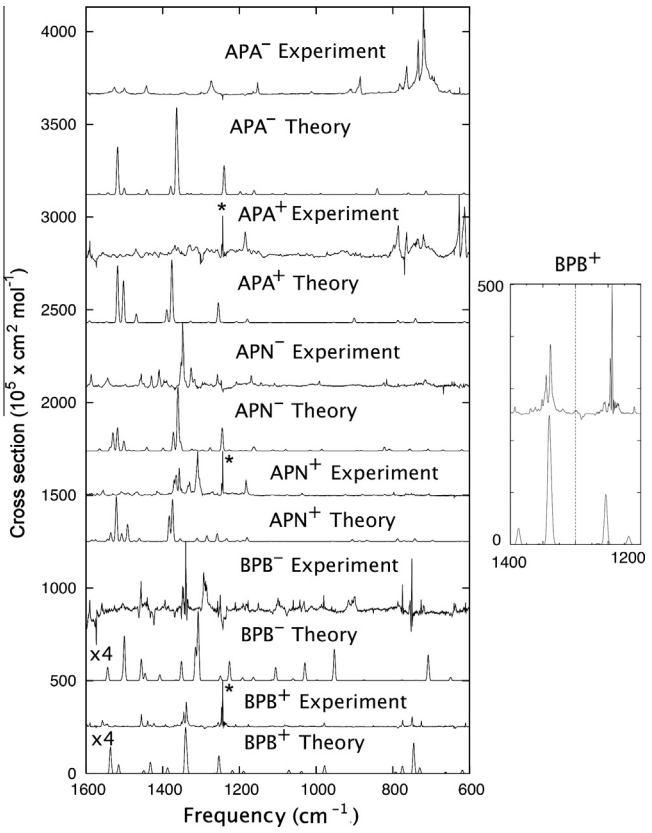

Fig. 7. Experimental mid-IR and theoretical vibrational spectra for the ions of BPB, APN, and APA. Theoretical values for BPB have been multiplied by a factor of 4 to allow examination of the spectral features. The experimental cross sections have been scaled so that the experimental maximum is equal to the theoretical value for the same ion and the spectra are offset for clarity. An NO_2 photoproduct is marked with a "∗". The BPB^+ blowup on the right focuses on the band at 1300.1 cm^{-1} that is marked with a vertical line.

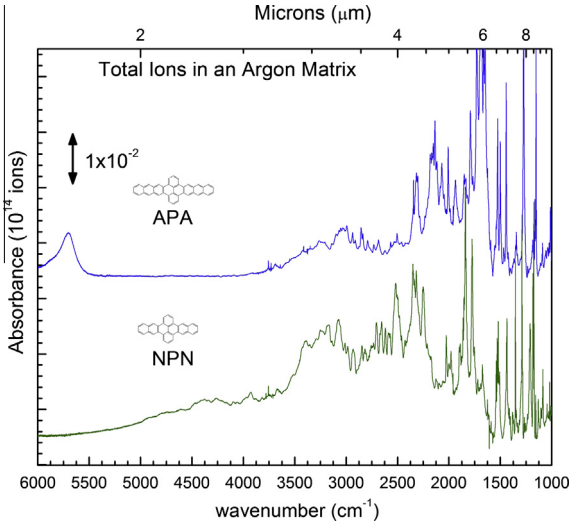

Fig. 8. The mid to near-IR spectra of APA and NPN ions in an argon matrix. Note the underlying electronic continuum stretching out to 4000 cm^{-1} for APA and past 5000 cm^{-1} for NPN. The spectra have been minimally baseline corrected with points around 5000 cm^{-1} and 650 cm^{-1} for APA and 6000 cm^{-1} and 650 cm^{-1} for NPN.

that are close in energy which results in some intensity sharing that makes weak modes stronger than they should be. There are also a few weak experimental bands where the only theory bands in the same region are forbidden. It is possible that these bands become allowed in the matrix or they correspond to combination or overtone bands, which are not included in the calculations. Excluding these few odd bands, one finds that the average absolute errors for the five molecules are 5.9 cm^{-1} for B3LYP and 8.1 cm^{-1} for BP86. The maximum errors are 29 and 25 cm^{-1} for B3LYP and BP86, respectively, while the second largest errors are 19 and 20 cm^{-1}. From the tables it is clear that the BP86 and B3LYP levels of theory are in good agreement for these systems, as found previously.

Fig. 2 shows the mid-infrared spectra of the dibenzopolyacene series from pyrene through APA. Fig. 2b displays what is commonly known as the CH out-of-plane or CH_{oop} region (500–1000 cm^{-1}). As emphasized by Hudgins and Allamandola [40] and Bauschlicher et al. [41], this range can typically be broken up into regions, with some overlap, in which the solo (one H on a ring), duo (two H atoms on the same ring), trio, and quartet hydrogen out-of-plane motions fall. The dibenzopolyacenes deviate somewhat from that typical trend. In the pyrene spectrum (lowest in Fig. 2b) the duo and trio hydrogen modes are clearly visible around approximately 845 and 710 cm^{-1}, with the trios falling some 30 cm^{-1} to the red of the normal range. However, when an additional aromatic ring is added creating BP, a molecule with duo, trio, and quartet CHoop motions, the spectrum only shows what appears to be duo and trio modes. For BPB, which contains only trio and quartet modes, this is even more evident as there is only one major band in this region of the spectrum. This unusual trend is broken for the remaining four dibenzopolyacenes, where the solo, trio, and quartet hydrogen modes are clearly visible in each spectrum and fall in ranges found for most neutral PAHs. Our quantum mechanical calculations reveal that the origin of this behavior is a coupling of the trio and quartet hydrogen modes in BPB. This coupling is broken with the addition of the solo hydrogen CH_{oop} motion in the larger systems.

The C–C and C–H in-plane vibrational motions for the dibenzopolyacene family are shown in the spectra of Fig. 2a. The most interesting spectral feature of this region is the dominance of a vibrational motion around 1440 cm^{-1}. This feature, absent in the pyrene molecule, is clearly present in BP and remains present through the largest dibenzopolyacene molecules. As Figs. 2 and 3 show, this feature increases in intensity with increasing dibenzopolyacene size, resulting in an intensity just shy of 100 km/mol for the APA molecule. In comparison, the regular polyacene molecules do not exhibit any such feature, although there is a small band (<5 km/mol) near 1450 cm^{-1} for pentacene and anthracene. Our calculations show that this vibrational mode is the result of the hydrogen atoms, especially the trio and quartet hydrogens, moving together along the long axis of the molecule inducing a dipole moment correlated with the length of the polyacene chain (see Fig. 4).

The experimental C–H stretching region of the dibenzopolyacenes is shown in Fig. 5a. As the figure shows, the pyrene C–H stretching region almost appears as a single band with the center slightly to the red of the C–H stretching modes in the other molecules. The spectrum of BP is dominated by a band around 3060 cm^{-1}. This band appears to be present in the other dibenzopolyacene spectra as well. As Fig. 5b shows, by substituting a deuterium atom in place of a hydrogen atom in our quantum mechanical calculations, the C–H stretching region can be deciphered. The calculated C–H spectrum for APA with no deuterium is composed of 4 separate bands, see Fig. 5b. Replacing the trio and quartet hydrogens with deuterium atoms, reveals the uncoupled solo band. Similarly, replacing the solo and quartet hydrogens or the solo and trio hydrogens with deuterium reveals the uncoupled trio or quartet bands. An inspection of these bands shows that the band furthest to the blue (3100 cm^{-1}) in the "all hydrogen" spectrum does not look like any of the individual bands. The bay

Table 1
The vertical excitation energies, in eV, and *f* values (given in parentheses) for the 5 lowest states of NPN as a function of level of theory. "TD" indicates the level of theory used in the TD-DFT calculations while "Geom" indicates the level of theory used in the geometry optimization.

	$\Delta E(f)$	$\Delta E(f)$	$\Delta E(f)$	$\Delta E(f)$	$\Delta E(f)$	$\Delta E(f)$
Neutral						
TD	B3LYP/4-31G	B3LYP/4-31G	B3LYP/6-31G*	BP86/4-31G	BP86/6-31G*	BLYP/6-31G*
Geom	B3LYP/4-31G	BP86/4-31G	B3LYP/6-31G*	BP86/4-31G	BP86/6-31G*	BLYP/6-31G*
	3.47(0.001)	3.40(0.001)	3.37(0.000)	2.72(0.000)	2.63(0.000)	2.62(0.000)
	3.48(0.000)	3.42(0.000)	3.40(0.001)	2.77(0.004)	2.68(0.003)	2.67(0.004)
	3.55(0.029)	3.48(0.029)	3.46(0.028)	2.94(0.000)	2.86(0.000)	2.84(0.000)
	3.57(0.000)	3.50(0.000)	3.47(0.000)	2.97(0.001)	2.90(0.001)	2.88(0.001)
	3.68(0.004)	3.62(0.004)	3.55(0.001)	3.18(0.028)	3.07(0.025)	3.05(0.024)
Cation						
	0.34(0.063)	0.34(0.062)	0.33(0.060)	0.29(0.028)	0.28(0.025)	0.28(0.026)
	0.37(0.000)	0.36(0.000)	0.37(0.000)	0.33(0.000)	0.34(0.000)	0.33(0.000)
	1.30(0.001)	1.28(0.001)	1.26(0.002)	1.21(0.000)	1.19(0.000)	1.17(0.000)
	1.33(0.000)	1.31(0.000)	1.29(0.000)	1.23(0.001)	1.19(0.001)	1.18(0.001)
	1.97(0.142)	1.94(0.141)	1.93(0.131)	1.75(0.121)	1.71(0.112)	1.69(0.111)
Anion						
	0.25(0.033)	0.23(0.028)	0.29(0.043)	0.31(0.026)	0.35(0.032)	0.34(0.030)
	0.42(0.007)	0.40(0.006)	0.43(0.007)	0.48(0.005)	0.50(0.005)	0.49(0.005)
	1.38(0.000)	1.37(0.000)	1.34(0.000)	1.30(0.158)	1.27(0.000)	1.26(0.000)
	1.39(0.203)	1.38(0.202)	1.37(0.189)	1.30(0.000)	1.28(0.147)	1.27(0.146)
	2.04(0.000)	2.03(0.000)	2.00(0.000)	1.90(0.000)	1.86(0.000)	1.84(0.000)

Table 2
The vertical excitation energies, in eV, and *f* values (given in parentheses) for the 5 lowest states. The TD-B3LYP approach is used at the B3LYP optimized geometry. The corresponding polyacene is also given using the letter notation in Fig. 1.

$\Delta E(f)$	$\Delta E(f)$	$\Delta E(f)$	$\Delta E(f)$	$\Delta E(f)$	$\Delta E(f)$	$\Delta E(f)$	$\Delta E(f)$
Neutral							
P	BP	BPB	NPB	NPN	APB	APN	APA
3.82(0.28)	3.75(0.00)	3.77(0.00)	3.47(0.00)	3.47(0.00)	2.84(0.03)	2.84(0.03)	2.75(0.00)
3.87(0.00)	3.87(0.18)	3.91(0.08)	3.61(0.01)	3.48(0.00)	3.14(0.02)	3.15(0.00)	2.82(0.03)
4.59(0.00)	4.38(0.26)	4.09(0.00)	3.89(0.29)	3.55(0.03)	3.54(0.60)	3.18(0.01)	2.84(0.04)
4.77(0.00)	4.48(0.13)	4.42(0.61)	3.95(0.04)	3.57(0.00)	3.57(0.00)	3.22(0.01)	2.88(0.00)
4.78(0.29)	4.64(0.00)	4.43(0.00)	4.00(0.01)	3.68(0.00)	3.70(0.00)	3.53(0.10)	3.18(0.02)
I	J	K	L	M	M	N	O
4.60(0.07)	3.39(0.07)	2.59(0.06)	2.03(0.05)	1.62(0.04)	1.62(0.04)	1.31(0.03)	1.07(0.03)
4.62(0.00)	4.00(0.00)	3.61(0.01)	3.03(0.00)	2.50(0.00)	2.50(0.00)	2.09(0.00)	1.77(0.00)
5.94(0.00)	4.68(0.00)	3.73(0.00)	3.34(0.02)	2.79(0.00)	2.79(0.00)	2.35(0.00)	2.00(0.00)
6.25(1.24)	5.13(0.00)	4.11(0.00)	3.36(0.00)	3.15(0.03)	3.15(0.03)	3.01(0.05)	2.62(0.00)
6.52(0.00)	5.68(0.00)	4.84(0.00)	4.10(0.00)	3.50(0.00)	3.50(0.00)	3.01(0.00)	2.91(0.07)
Cation							
P	BP	BPB	NPB	NPN	APB	APN	APA
1.24(0.00)	0.75(0.00)	0.59(0.00)	0.19(0.01)	0.34(0.06)	0.40(0.00)	0.25(0.04)	0.23(0.06)
1.84(0.03)	1.49(0.01)	0.84(0.01)	0.56(0.02)	0.37(0.00)	0.70(0.02)	0.52(0.00)	0.76(0.00)
2.17(0.01)	1.58(0.07)	1.41(0.12)	1.30(0.02)	1.30(0.00)	1.45(0.15)	1.30(0.06)	1.30(0.00)
2.78(0.02)	2.49(0.00)	1.82(0.00)	1.45(0.07)	1.33(0.00)	1.57(0.00)	1.48(0.00)	1.62(0.00)
3.10(0.27)	2.68(0.02)	2.62(0.03)	2.20(0.04)	1.97(0.14)	2.07(0.00)	1.81(0.16)	1.64(0.00)
I	J	K	L	M	M	N	O
1.16(0.00)	1.58(0.00)	1.74(0.17)	1.30(0.01)	0.96(0.01)	0.96(0.01)	0.69(0.01)	0.48(0.01)
2.21(0.05)	1.99(0.11)	1.76(0.01)	1.54(0.25)	1.37(0.33)	1.37(0.33)	1.16(0.00)	0.86(0.00)
3.04(0.01)	2.38(0.01)	1.86(0.00)	1.94(0.00)	1.54(0.00)	1.54(0.00)	1.23(0.42)	1.11(0.52)
3.48(0.00)	3.07(0.00)	2.66(0.00)	2.15(0.00)	2.17(0.00)	2.17(0.00)	1.82(0.00)	1.49(0.00)
3.57(0.00)	3.24(0.06)	2.82(0.00)	2.53(0.00)	2.28(0.00)	2.28(0.00)	2.04(0.00)	1.66(0.00)
Anion							
P	BP	BPB	NPB	NPN	APB	APN	APA
1.26(0.00)	0.73(0.01)	0.63(0.01)	0.18(0.00)	0.25(0.03)	0.38(0.00)	0.19(0.03)	0.20(0.04)
1.75(0.02)	1.38(0.01)	0.65(0.00)	0.42(0.00)	0.42(0.01)	0.66(0.02)	0.47(0.00)	0.88(0.01)
2.24(0.00)	1.51(0.06)	1.34(0.10)	1.30(0.00)	1.38(0.00)	1.42(0.15)	1.29(0.06)	1.50(0.27)
3.05(0.29)	2.64(0.00)	1.72(0.00)	1.41(0.13)	1.39(0.20)	1.55(0.00)	1.46(0.00)	1.67(0.00)
3.06(0.01)	2.93(0.01)	2.91(0.02)	2.34(0.05)	2.04(0.00)	2.03(0.01)	1.77(0.16)	1.75(0.00)
I	J	K	L	M	M	N	O
1.22(0.00)	1.68(0.00)	1.69(0.02)	1.24(0.01)	0.90(0.01)	0.90(0.01)	0.64(0.01)	0.43(0.01)
2.34(0.06)	2.15(0.12)	1.90(0.20)	1.67(0.28)	1.49(0.37)	1.49(0.37)	1.22(0.00)	0.91(0.00)
3.24(0.01)	2.33(0.02)	1.99(0.00)	2.05(0.00)	1.61(0.00)	1.61(0.00)	1.33(0.47)	1.19(0.58)
3.29(0.00)	3.22(0.00)	2.75(0.00)	2.27(0.00)	2.27(0.00)	2.27(0.00)	1.87(0.00)	1.54(0.00)
3.72(0.00)	3.60(0.05)	3.06(0.00)	2.81(0.00)	2.38(0.00)	2.38(0.00)	2.10(0.00)	1.72(0.00)

region is known [41] to have a hydrogen-hydrogen interaction that shifts the band to the blue. So when the solo and trio bands are allowed to couple, the band furthest to the blue looks like the "all hydrogen" case. Adding the coupled solo and trio spectra to the quartet spectra is essentially the same as the "all hydrogen" case indicating that the quartet hydrogens (which are the major contributor to the C–H stretching occurring between 3060 and 3080 cm^{-1}) are weakly coupled to the solo hydrogen atoms.

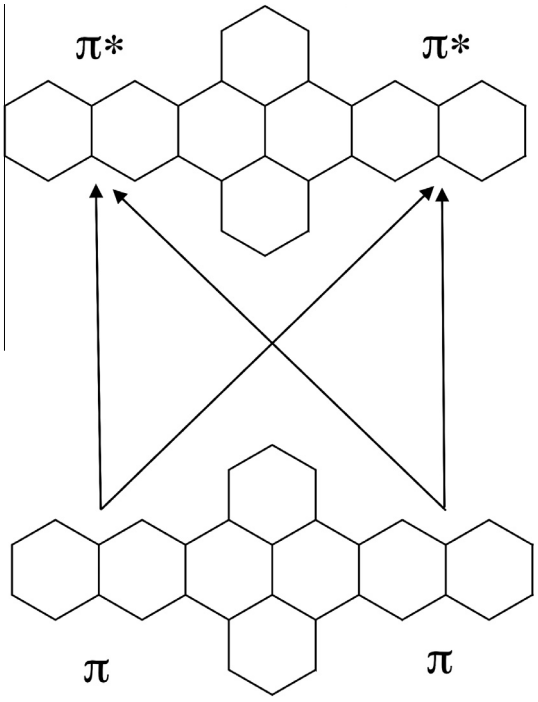

Fig. 9. An illustration of the excitations in a localized or fragment view. Namely, excitations from the π orbitals on the right and left hand side naphthalene units of the molecule to the π^* orbitals of each fragment.

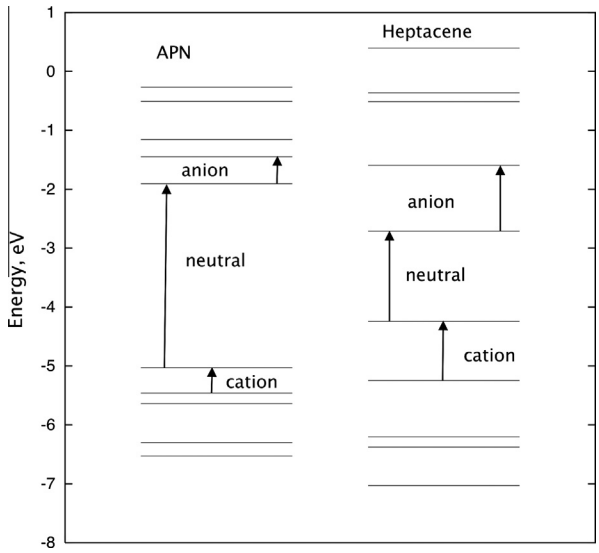

Fig. 10. The orbital energy levels for the five highest occupied and five lowest unoccupied orbitals for neutral APN and heptacene. The excitations for the neutral, cation, and anion are shown.

Vibrational spectra of the ions

In general, the experiments for the ions are more complex than those of the neutrals. In the UV irradiated Ar matrix experiments both cations and anions form and the addition of NO_2 is required to separate the cation spectra from that of the anion. Moreover, in both experiments the spectra of the neutral must be accounted for by subtraction from the matrix-isolated ionized spectra. Fig. 6 shows the data as collected, while Fig. 7 shows three examples where the anion spectra have been created by subtracting the Ar/NO_2 spectra from the Ar spectra. These spectra illustrate the complexity of analyzing the ion results.

In the Supplemental Tables, the cation intensities are computed assuming that there are 100% cations in the NO_2 doped Ar and 50% cations in the pure Ar matrix. If our assumptions are correct, the ratio of the cation band intensities in NO_2 doped Ar to those in pure Ar should be 1 to 1. If more cations than anions were formed in the pure Ar matrix, the ratio would be larger than 1, reaching an upper limit of 2, if no anions at all were formed in the photolyzed Ar matrix. However, as Table S6 shows, the ratio of the IR bands in the NO_2/Ar matrix can vary from 0.7 to 3.8 for the corresponding bands of BPB^+ isolated in Ar. Integration and analysis of the bands is complicated by the presence of photoproducts and by the presence of strong electronic transitions for the ionized dibenzopolyacenes that fall in the mid-IR. Unlike experiment, it is possible to completely separate the electronic and vibrational spectra using theory, and therefore it would appear that theory is ideally suited to better understand these complicated ions. However, it is important to realize that the same low-lying electronic states that cause problems in the experiments can also lead to computational problems. In this section we focus on using both theory and experiment to gain insight into the spectra of these species.

The spectra for three representative ions are shown in Fig. 7. The spectra of BPB are typical of small molecules where the lowest electronic transitions do not fall in the same region of the spectra as the vibrational bands. The spectra of APN are typical of our asymmetric XPY species, where the electronic transitions are expected to fall in the same region as vibrational bands, but appear to be so weak that they do not cause serious problems. The spectra of APA are typical of our large symmetric XPX species, where the strong electronic transitions fall in the same spectral region as the vibrational modes and produce, for example, the very strong bands in the 600–800 cm^{-1} region for both the APA anion and cation. From the magnitude of the bands, both total intensity and width, it is clear that these bands involve electronic transitions. In addition, the presence of a broad underlying continuum stretching out past 3000 cm^{-1} for NPN and APA ions (see Fig. 8) illustrates that these are not typical PAH spectra and supports the view that electronic transitions are occurring in the mid-IR. There are sharper bands superimposed on the broad bands that suggest that we are observing a vibrational progression in the excited state vibrational levels. That is, we are observing $(0,0,\ldots,0) \rightarrow (v'_1,0\ldots,0)$ transitions in addition to $(0,0,..,0) \rightarrow (0,0,\ldots,0)$. The very small difference between the bands suggests that we are exciting the very low frequency vibrational modes in the excited electronic state. We note however that these sharp features fall at positions consistent with our computed vibrational band positions, see Tables S6 to S12. This leads to the possibility that the sharp features are in fact ground state vibrational modes that grow dramatically in intensity by some coupling to the electronic transition. We are unable to differentiate between these two cases.

The spectra for the ions of BPB are shown in Fig. 7. We first focus on the cation. A line-by-line comparison (see Table S6) shows that the agreement between theory and experiment for band positions is good and is commonly 10 cm^{-1} or better. The sizeable band at 1235 cm^{-1} in the experimental spectra is due to a NO_2 photoproduct, which affects the overall scaling of the experimental spectra. However, even after accounting of this photoproduct, the experimental and theoretical intensities show some discrepancies. For example, the experimental bands in the 1500–1600 cm^{-1} region are weaker than those in the 1400–1500 cm^{-1} region, which is the opposite found in theory. There appears to be a band in experiment at 1300.1 cm^{-1} that has no good matching band in theory, with the nearest theory band being a weak band at 1265.4 cm^{-1}, see the blowup of this section of the BPB^+ spectra in Fig. 7. Considering that this band is much weaker than those nearby, it

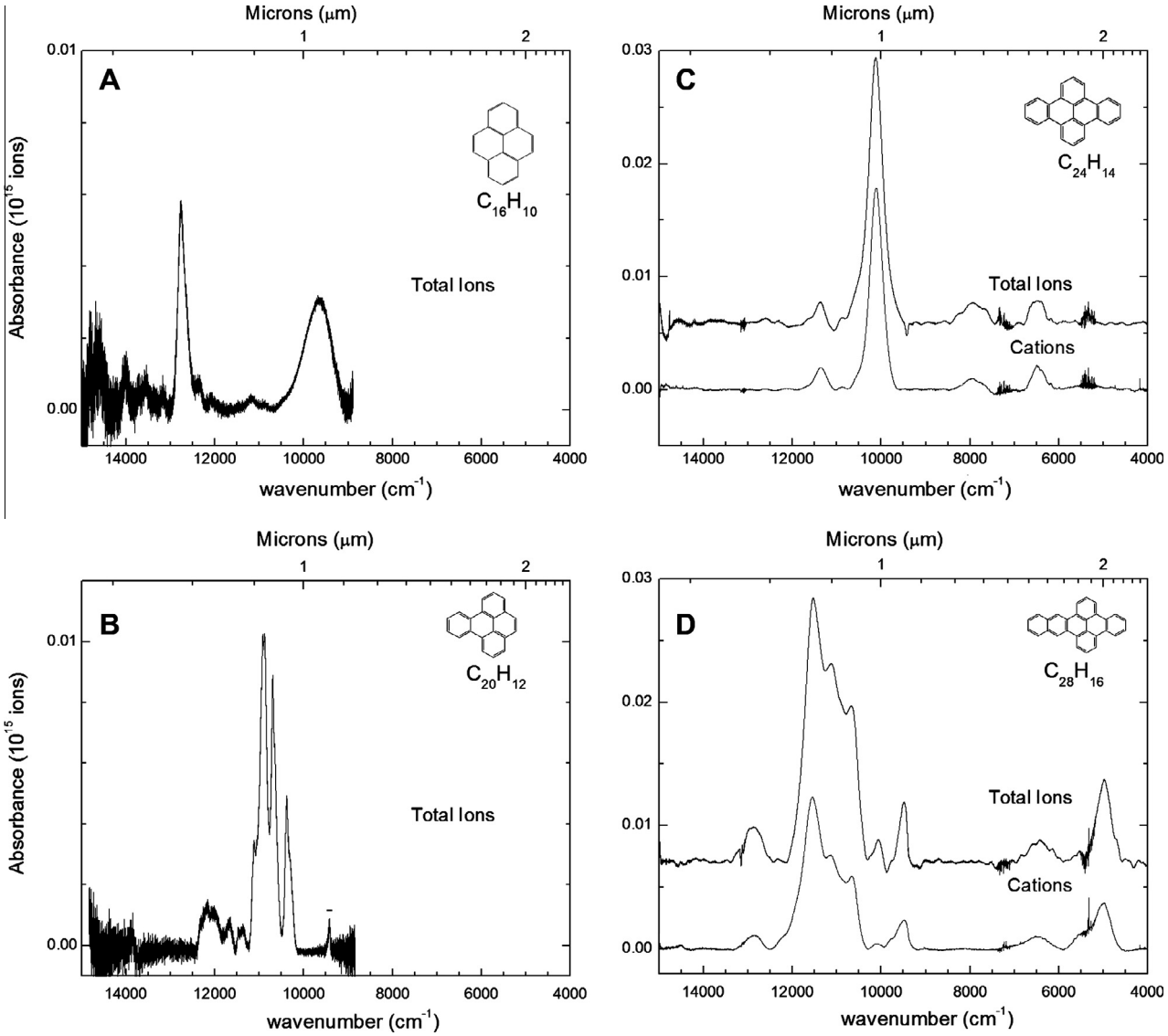

Fig. 11. NIR spectra of matrix-isolated radical cations and anions for P, BP, BPB, and NPB, which are in panels A, B, C, and D, respectively. In all cases the lower spectrum is for the cation, while the upper spectrum is for the anions and cations. Note the accumulation of bands around the 10,000 cm^{-1} (1 μm) region. The P and BP are included for completeness and are taken from Mattioda et al. [21].

is possible that it is an overtone or a combination band. However, we note that there is a strong anion band in theory at 1307.6 cm^{-1}. This suggests that some anions may remain in the NO_2 doped experiments, which could affect the intensities of other bands as well, for example the band at 1455 cm^{-1}. A comparison (Table S7) between theory and experiment for BPB^- finds agreement of similar quality excluding a strong band in experiment at 915.6 cm^{-1}, where the nearest strong band in theory falls at 952.4 cm^{-1}. This suggests that while most of the band positions are accurate to about 10 cm^{-1}, one band has an error of 36.8 cm^{-1}. Thus, for BPB, where there are no low-lying excited electronic states, there is reasonable agreement between theory and experiment for the ions, with errors that are only slightly larger than found for the neutrals.

The spectra for the ions of APN are shown in Fig. 7. As with BPB, the experimental and theoretical band positions agree reasonably well, but there are discrepancies for the intensities. Again there is the pronounced difference for the intensities in the 1500–1600 cm^{-1} region. The experimental values for this region seem to be small compared with the intensity in other regions of the spectra as compared with other PAH cations. The experimental anion spectrum shows some features in the 600–800 cm^{-1} region and we are unable to determine if this is noise in our spectra or is an indication of weak electronic transitions.

The theoretical and experimental spectra for the APA ions are shown in Fig. 7. There is no agreement to speak of as the experimental spectra contain both electronic and vibrational transitions, while theory contains only vibrational transitions. In Tables S19 and S20 the theoretical and experimental vibrational band positions and intensities for the cation and anion, respectively, are compared. In spite of the strong electronic transitions, the agreement for the vibrational band positions is acceptable, with several bands showing a 30 cm^{-1} difference. The agreement of the intensities is qualitative. We suspect that part of the differences arise from the use of BP86, which is less reliable than the B3LYP approach that we typically use, and part arises from the complexity of extracting vibrational information from the much stronger electronic transitions.

NPB^- is another interesting case, where theory has many more bands than experiment. We suspect that much of this difference arises from problems with observing all of the bands in experiment, since the experimental spectra has far fewer bands than typically found for a PAH of this size.

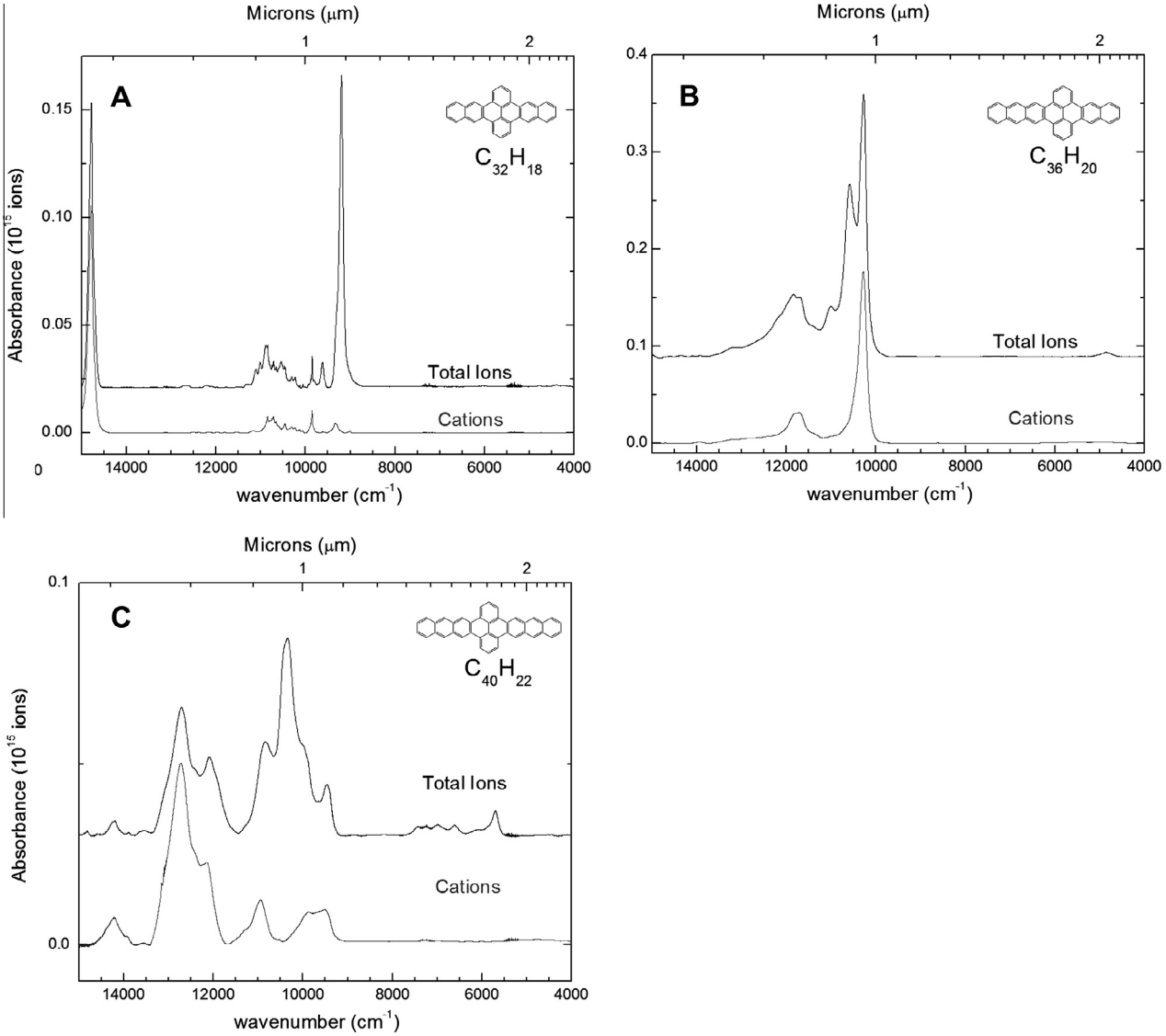

Fig. 12. NIR spectra of matrix-isolated radical cations and anions for NPN, APN, and APA, which are in panels A, B, and C, respectively. In all cases the lower spectrum is for the cation, while the upper spectrum is for the anions and cations. Note the accumulation of bands around the 10,000 cm^{-1} (1 μm) region.

A comparison of theory and experiment shows that there is good agreement for the band positions, but that some experimental bands seem to be obscured. This is especially true for those ions with electronic transitions in the IR. On the basis of the agreement for the bands that can be observed clearly in experiment, we believe that the best estimate for the vibrational IR spectra for these ions is probably obtained from theory. While the band positions agree well, we must note that theory and experiment can differ significantly for the intensity. It should also be noted that one cannot generate a synthetic absorption spectrum that agrees with experiment because we cannot accurately describe the electronic transitions nor the coupling of the electronic and vibrational excitations. While theory does not directly suffer from the low-lying excited states, it indirectly suffers from the low-lying excited states as indicated by the failure of B3LYP for these ions and even the failure of BP86 for NPB^+. While theory gives the best overall description of the vibrational bands for these ions, if one is interested in some specific transitions, it is best to use the experimental results for accurate band positions. The experiments also yield information on the overtone and combination bands between 1600 and 3000 cm^{-1}.

B3LYP vertical excitation energies

TD-DFT offers an efficient way to study electronic excitations from the ground state. Hybrid functionals are commonly believed to be more accurate than non-hybrid functionals, but even the hybrids are probably accurate to only about 0.3 eV. This is not a problem since the main goal of TD-DFT calculations is not to assign the observed electronic transitions, but rather to find the trends as a function of the size and shape of the dibenzoacenes. However, before considering the trends, we report on some calibration calculations for NPN, see Table 1. We use the B3LYP and BP86 functionals that were used to study the vibrational frequencies and the BLYP functional [31,42] that was used in the study of Weisman et al. [20]. Note that the BLYP results are slightly different than those previously reported because the current work uses the more stable nonplanar geometry and the forbidden states are reported as well as the allowed. A comparison of the allowed transitions in Table 1 with those given in Weisman et al. [20] shows the change in geometry hardly affects the excitation energies.

A comparison of columns 1 and 2 (B3LYP/4-31G//B3LYP/4-31G and B3LYP/4-31G//BP86/4-31G) shows that the use of the B3LYP

Table 3
Electronic transitions for BPB and NPB. The excitation energy, ω, is in cm^{-1}, the intensities, A, are in km/mol, while the oscillator strength, *f*, is dimensionless. The transitions for the analogous tetracene and pentacene are also given.

BPB						Tetracene [21]		
Argon matrix			NO_2 doped matrix			Cation		
ω	*A*	*f*	ω	A	*f*	ω	*A*	*f*
6500[a]	9362.6	1.75×10^{-3}	6495	284789	5.33×10^{-3}	11520	56000	0.0106
7946[b]	7689.2	1.44×10^{-3}	7971	24886	4.65×10^{-3}	11900	43000	0.008
10123[c]	143254.6	2.68×10^{-2}	10118	291097	5.44×10^{-2}	12170	890	0.00017
10895[d]	962.6	1.80×10^{-4}	10891	719	1.35×10^{-4}	12240	1200	0.00022
11374[e]	6663.8	1.25×10^{-3}	11365	19709	3.69×10^{-3}	12470	7400	0.001
						12910	3200	0.0006
						13060	3300	0.00062
						13160	vw	vw
						13420	13000	0.0025
						13680	2400	0.0045
NPB						Pentacene [21]		
4985[f]	62790	1.17×10^{-2}	5010	39089	7.31×10^{-3}	8940	140	0.000026
6430[g]	13979	2.61×10^{-3}	6445	10394	1.94×10^{-3}	9010	310	0.000058
9495[h]	16485	3.08×10^{-3}	9505	9326	1.74×10^{-3}	9890	850	0.00016
10050[i]	3816	7.14×10^{-4}	10107	961	1.80×10^{-4}	10150	9600	0.0018
11125[j]	284064	5.31×10^{-2}	11125	200020	3.74×10^{-2}	10470	84000	0.0158
12890[k]	550	1.03×10^{-4}	12857	4310	8.06×10^{-4}	10900	570	0.00011
12900[l]	18623	3.48×10^{-3}				11000	170	0.000032
						11100	250	0.000047
						11370	250	0.000047
						11870	32000	0.006
						13280	vw	vw
						13410	vw	vw

[a] Very broad 600 cm^{-1} wide band, weak, shifts to 6495 cm^{-1} for cation only.
[b] Weak, broad 900 cm^{-1} wide band.
[c] Most intense band, shifts to 10,113 cm^{-1} for cation only.
[d] Very small band, shoulder on 10,123 cm^{-1} band. Seems to shift slight to 10,885 cm^{-1} in cation only data.
[e] Shifts to 11,364 cm^{-1} in cation only data.
[f] Broad band 1000 cm^{-1} wide, weak shoulder around 5500 cm^{-1}.
[g] Weak broad band, 900 cm^{-1} wide, cation band centered around 6500 cm^{-1}.
[h] Shoulder at 9785 cm^{-1}.
[i] Weak band, cation band weaker and shifted to 10,120 cm^{-1}.
[j] Broad band composed of three bands centered at 11,550, 11,125 and 10,640 cm^{-1}.
[k] Weak band.
[l] Argon data integrated after baseline correction.

or the BP86 geometries makes only a very small difference. Thus while the B3LYP does not yield reliable vibrational frequencies for the ions, the geometries are very similar to those from the BP86 functional. A comparison of columns 1 and 3 (B3LYP/4-31G//B3LYP/4-31G and B3LYP/6-31G*//B3LYP/6-31G*) and of 4 and 5 (BP86/4-31G//BP86//4-31G vs BP86/6-31G*//BP86/6-31G*) shows that using the small 4-31G basis set has an average absolute and maximum difference of 0.05 and 0.13 eV, respectively, in the excitation energies compared with the larger 6-31G* basis set. Clearly, the smaller basis set can be used to illustrate the trends. A comparison of the last two columns shows that BP86 and BLYP, the two non-hybrid functionals, yield very similar results; an average absolute and maximum difference of 0.05 and 0.11 eV, respectively. The B3LYP results differ somewhat from the BP86 and BLYP values. For the neutrals the average absolute and maximum differences with the non-hybrids are 0.58 and 0.74 eV, respectively. The analogous differences for the ions are smaller, being 0.08 and 0.22 eV. On the basis of these calibrations and the general preference for hybrids in TD-DFT calculations we use the B3LYP/4-31G//B3LYP/4-31G approach to study all of the systems.

These species can be viewed as being composed of three components: the central pyrene (P) and the left and right wings (X and Y). An understanding of the electronic excitations of XPY starts with the consideration of the π to π^* excitation energy of the individual components. In ascending order, the B3LYP excitation energies (given in parentheses) are: anthracene (3.39) < pyrene (3.82) < naphthalene (4.60) $\ll$ benzene (5.64).

The XPX π and π^* orbitals are either symmetric or asymmetric about the short axis of the molecule. While the XPX calculations are performed with the symmetry-adapted molecular orbitals, it is probably not the best way to compare the XPX and the less symmetric XPY species. The plus and minus combinations of the XPX π or π^* orbitals yields orbitals that are localized on the left and right sides of the XPX molecule, which are more similar to the orbitals found for the XPY species and are consistent with a fragment view of the excitations. Therefore we sometimes discuss the XPX excitations in terms of localized orbitals.

The five lowest excited states for pyrene range from 3.82 to 4.78 eV, see Table 2. Because the lowest excitation energy in benzene is almost 2 eV higher than in pyrene, the addition of the benzene wing or wings in BP and BPB does not make a significant change in the two lowest excitation energies. Since the excitation energies for the third through fifth states of pyrene (4.59, 4.77, and 4.78 eV) are becoming closer to the excitation energy of benzene, some benzene character mixes in to the wave function for the higher states of BP and BPB. Thus, while the lowest excitation energies for P, BP, and BPB differ by up to 0.07 eV, the fifth state excitation energies differ by up to 0.35 eV, with the expected ordering P > BP > BPB.

For NPB and NPN more mixing of the components occurs as they are closer in energy. The lowest excitation energies for NPB and NPN are very similar, and the excitation involves orbitals that are a mixture of the pyrene and naphthalene components. The excitation energies rise more quickly for NPB as the higher energy benzene component is forced to mix in. For NPN, the five lowest states have rather similar energies and an inspection of the excitations and localized orbitals suggests that they correspond to π to π^* on the pyrene and π to π^* excitations on the naphthalene units. In a

localized or fragment view, the four naphthalene centered excitations can be viewed as excitations originating from the right or left hand side naphthalene π orbital terminating in either the right or left hand side naphthalene π^* orbitals, see Fig. 9.

The lowest excitation energies for APB, APN, and APA are very similar and the orbitals involved appear to be mostly π to π^* on the anthracene component, which is consistent with anthracene having the lowest-lying excited state. The second state in APB appears to be mostly π to π^* on the pyrene. The third through fifth state excitation energies are similar for APB and NPN, this might appear strange until one realizes that APB and NPN are the same size, just one C_6 ring switches sides. APA has 4 states with very similar energies corresponding to π to π^* excitations on the anthracenes.

The excitation energies for the ions are much smaller than for the neutrals. The origin of this difference is illustrated in Fig. 10, where the orbital energy levels for APN are given. In the cation, the highest occupied molecular orbital (HOMO) of the neutral is now singly occupied, so the lowest excitation in the cation is from the HOMO−1 to the HOMO. Since the HOMO and HOMO−1 are very close in energy for these molecules, the excitation energy is quite small. We note that the HOMO−2 is close to the HOMO−1, so there is more than one low-lying excited state. For the anion, the extra electron occupies what was the lowest unoccupied orbital (LUMO) in the neutral. Since the LUMO and LUMO+1 orbitals are close in energy for these molecules, the excitation energy is small for the anion. There is a general trend of decreasing excitation energy for the ions with increasing molecular size. The similar energies for the HOMO and HOMO−1 and LUMO and LUMO+1 are consistent with the low-lying state(s) that cause the B3LYP frequencies to be unreliable.

In Table 1 we also include the polyacene of the same length for comparison. We first note that the lowest excitation for neutral pyrene is smaller than for naphthalene, which is consistent with pyrene being a larger molecule. However, for the rest of the neutral series adding the two benzene rings increases the excitation energy and the size of the effect increases with increasing length; the difference between APA and octacene being 1.68 eV. While adding the benzene rings to the parent polyacene increases the excitation energy for the neutrals, it actually decreases the excitation energies for ions (excluding pyrene), which is consistent with the idea that the larger the molecule, the smaller the lowest excitation energy. The origin of this difference between the dibenzoacene and polyacenes has been discussed by Weisman et al. [20]

Table 4
Electronic transitions for NPN in the NIR. The excitation energy, *E*, is in cm^{-1}, the intensities, *A*, are in km/mol, while the oscillator strength, *f*, is dimensionless. The analogous hexacene is also reported, including theoretical excitation energies (Th).

NPN						Hexacene [13]							
Argon matrix			NO_2 doped matrix			Anion				Cation			
ω	*A*	*f*	ω	*A*	*f*	ω	*A*	*f*	Th	ω	*A*	*f*	Th
9007[a]			9008	574	1.07×10^{-4}	not observed			6830	6422	53476	0.01	7369
9195[b]	247164	4.62×10^{-2}								9183	1636364	0.306	10870
9343[c]			9342	7104	1.33×10^{-3}					9390			
9613[d]			9614	390	7.29×10^{-5}								
9620[e]	14286	2.67×10^{-3}											
9719[f]			9717	71	1.33×10^{-5}								
9854[g]	9674	1.81×10^{-3}	9855	7981	1.49×10^{-3}	9900	1860963	0.35	11848				
10058[h]	536	1.00×10^{-4}	10061	360	6.74×10^{-5}								
10129[h]	338	6.32×10^{-5}	10130	642	1.20×10^{-4}								
10234[h]	4795	8.97×10^{-4}	10236	978	1.83×10^{-4}								
10310[h]	6781	1.27×10^{-3}	10314	1201	2.25×10^{-4}								
10450[i]	4865	9.10×10^{-4}	10452	1939	3.62×10^{-4}								
10472[j]	3904	7.30×10^{-4}	10471	1936	3.62×10^{-4}								
10542[k]	19334	3.62×10^{-3}	10615	2845	5.32×10^{-4}					10560			
10658[l]	5873	1.10×10^{-3}	10661	2946	5.51×10^{-4}								
10716[m]	7254	1.36×10^{-3}	10717	12731	2.38×10^{-3}								
10745[n]	4291	8.02×10^{-4}	10745	2886	5.40×10^{-4}								
10790[h]			10790	3678	6.88×10^{-4}								
10850[o]	19696	3.68×10^{-3}	10849	6053	1.13×10^{-3}								
10891[p]	23939	4.48×10^{-3}											
11012[q]	11708	2.19×10^{-3}											
11110[p]	11139	2.08×10^{-3}	11178	903	1.69×10^{-4}								
11328[q]	2887	5.40×10^{-4}				11235							
14786[r]	240223	4.49×10^{-2}	14790	176952	3.31×10^{-2}								

[a] Cation band, small shoulder at 9007 cm^{-1} in Argon matrix.
[b] Very strong anion band, shoulders at 9310 and 9340 cm^{-1}.
[c] Cation band with shoulders at 9456, 9304 and 9188 cm^{-1}.
[d] Cation band with side band at 9564 and a shoulder at 9646 cm^{-1}.
[e] Gaussian shaped.
[f] Small, weak band.
[g] Very sharp band, broad base with side bands at 9810, 9885, 9908 and 9944 cm^{-1}.
[h] Cation band part of broad complex of numerous small bands.
[i] Cation band part of broad complex of numerous bands; this band and the one at 10,472 cm^{-1} comprise a doublet.
[j] Cation band part of broad complex of numerous bands; this band and the one at 10,450 cm^{-1} comprise a doublet.
[k] Anion, broad, part of broad complex of numerous small bands, side band at 10,610 cm^{-1}.
[l] Cation band with shoulder at 10,614 cm^{-1}, part of broad complex of numerous small bands.
[m] Cation band with side band at 10,745 cm^{-1}, part of broad complex of small bands.
[n] Cation band with side band at 10,716 cm^{-1}, part of broad complex of small bands.
[o] Cation band, part of broad complex of small bands; this band and the one at 10,891 cm^{-1} comprise a doublet.
[p] Anion band, part of broad complex of small bands.
[q] Part cation, part anion; cation component split into 11,300 and 11,365 cm^{-1}.
[r] Cation band, on the edge of our detector range.

and is shown in Fig. 10. The difference in orbital energy levels is very clear. The HOMO–LUMO gap is much smaller for the polyacenes, which leads to smaller excitation energies for the neutrals. However, the HOMO–HOMO−1 and LUMO–LUMO+1 gaps are much larger for the polyacenes, so the excitation energies are much larger for the polyacene ions than for the dibenzoacenes.

A comparison of NPN, APB, and hexacene shows that the addition of the benzene rings and their position all affect the excitation energies. This leads us to speculate that one could exercise a great deal of control on the electronic spectra of polyacene derivatives by the judicious placement of additional benzene side groups.

Experimental electronic spectra of the ions

We break the discussion of the electronic spectra into two ranges, the mid-IR and the near IR (NIR), with the dividing line being about 4000 cm^{-1}. In the mid-IR the electronic transitions overlap with the vibrational transitions, while the NIR region of the spectra is devoid of vibrational transitions and therefore we can identify the transitions as being electronic in origin.

In the mid-IR spectra, shown in Fig. 6, the spectra of the symmetric NPN and APA ions are divided by a factor of 50, while the less symmetric APN is divided by only 10. Clearly the symmetric species show stronger electronic transitions than the asymmetric species in the mid-IR. The computed oscillator strengths (f) for the lowest states of NPB^+ and NPN^+ are 0.01 and 0.06, while those for APB^+, APN^+, and APA^+ are 0.00, 0.04, and 0.06, respectively. The value for the anions are: 0.00(NPB^-), 0.03(NPN^-), 0.00(APB^-), 0.03(APN^-), and 0.04(APA^-). NPN and APB are the same size and the symmetric NPN has a larger f value than the asymmetric APB. The theoretical f values show that size plays a role, as the APN^- has the same value as NPN^-. While theory yields stronger electronic transitions for the symmetric species, the effect appears to be smaller than found in experiment.

Table 5
Electronic transitions for APN. The excitation energy, E, is in cm^{-1}, the intensities, A, are in km/mol, while the oscillator strength, f, is dimensionless. The analogous heptacene is also reported, including theoretical excitation energies (Th).

APN						Heptacene [13]							
Argon matrix			NO_2 doped matrix			Anion				Cation			
ω	A	f	ω	A	f	ω	A	f	Th	ω	A	f	Th
4858[a]	23700	4.43×10^{-3}				not observed			4759	4686	48128	0.01	4589
10275[b]	816243	1.53×10^{-1}	10281	595099	1.11×10^{-1}	8680	2379679	0.45	10613	8013	2090909	0.39	7849
10585[c]	728729	1.36×10^{-1}				100091				9200			9017
11012[q]	106088	1.98×10^{-2}								9434			9250
11836[d]	413568	7.73×10^{-2}	11775	146451	2.74×10^{-2}								
13220	9556	1.79×10^{-3}											
13929[e]			13929	3178	5.94×10^{-4}								

[a] Anion band.
[b] Cation band, shifted to 10,280 cm^{-1} in NO_2 doped matrix, anion side bands at 10,585 and 11,012 cm^{-1}.
[c] Anion band.
[d] Mixed cation and anion band. Both have shoulder around 11,360 cm^{-1}. Argon data has broader band with side bands at 11,695, shoulders at 12,215 cm^{-1}. Center shifted to 11,775 cm^{-1} from Ar data, double peak at 11,700 and at 11,835 cm^{-1}.
[e] Very weak.

Table 6
Electronic transitions for APA in NIR. The excitation energy, E, is in cm^{-1}, the intensities, A, are in km/mol, while the oscillator strength, f, is dimensionless. The analogous octacene is also reported.

APA						Octacene [16]	
Argon matrix			NO_2 doped matrix			Anions + cations	
ω	A	f	ω	A	f	ω	A
			4604	1885	3.53×10^{-4}		
5704[a]	27279	5.10×10^{-3}					
6100[a]	4560	8.53×10^{-4}					
6615[b]	8468	1.58×10^{-3}				6775	Strongest
6690	13551	2.53×10^{-3}					
7245	6632	1.24×10^{-3}				7358	
7740[c]	8577	1.60×10^{-3}					
9475[d]	65836	1.23×10^{-2}	9716	27540	5.15×10^{-3}		
10342[a]	519183	9.71×10^{-2}					
10840[e]	176317	3.30×10^{-2}	10950	17061	3.19×10^{-3}		
12090[f]							
12100[g]	190153	3.56×10^{-2}	12100	[h]		12407	
12711[i]	457146	8.55×10^{-2}	12740	224487	4.20×10^{-2}	13947	
14220[j]	16915	3.16×10^{-3}	14211	18257	3.41×10^{-3}	14925	
						19881	
						20450	

[a] Anion band.
[b] Anion bands, part of a complex of four bands.
[c] Cation and anion bands not separated out.
[d] Cation band with side band at 9870 cm^{-1}.
[e] Mix cation and anion band. Center shifts from 10,840 total ions to 10,950 cm^{-1} in cation.
[f] Mixed cation and anion band. Center around 12,090 cm^{-1} in total ion form, becomes a shoulder to 12,740 cm^{-1} band in cation data.
[g] Cation band, broad side band to 12,740 cm^{-1}.
[h] Included with the 12,740 cm^{-1} band intensity for NO_2.
[i] Cation band, shifts to 12,740 cm^{-1} in cation data. Has shoulder at 12,400 cm^{-1}.
[j] Cation band.

The individual spectra in the NIR are shown in Figs. 11 and 12 with the lower spectrum, measured in the NO_2-doped argon matrix, being due to the cation bands and the upper spectrum, measured in the argon matrix, containing both cation and anion transitions. A summary of the individual band areas and positions is given in Tables 3–6 along with the analogous polyacene molecule.

There are several interesting items to note in the spectra themselves. Despite the unique mid-IR electronic transitions for the radical cations and anions, the dibenzopolyacene NIR spectra closely resemble that of the other PAHs [21] and the PANHs (Polycyclic Aromatic Nitrogen Heterocycles) [43] that we have investigated. They are characterized by most of the intense NIR electronic features clustering around 1 μm (10,000 cm^{-1}). The smallest two members of this series (BPB and NPB) exhibit little, if any, radical anion bands upon photolysis, similar to that observed for other smaller PAHs [21]. This is probably related to the smaller electron affinities for small PAHs compared with larger PAHs. The three larger dibenzopolyacenes (NPN, APN, and APA) contain intense, radical anion bands in addition to the radical cation bands (Compare the upper and lower spectra in Figs. 11 and 12).

The band positions in the NIR for the dibenzopolyacenes and the analogous polyacenes are compared in Tables 3–6. For all of these systems many bands have been found. These need not all correspond to single 0–0 electronic transitions, in fact, many of the closely spaced lines probably correspond to overlapping vibronic transitions. Therefore, we focus on the position of the strongest band.

There does not appear to be a strong correlation between these two series. For the BPB cation vs tetracene cation, the very strong transition shifts up from 10,123 to 11,900 cm^{-1}, while for NPB^+ vs $pentacene^+$ the very strong band shifts down from 11,250 to 10,470 cm^{-1}. For NPN^+ vs $hexacene^+$ and APN^+ vs $heptacene^+$ the strongest transition shifts down, while for NPN^- and APN^- it is a shift up. For octacene, the cation and anion spectra are not separated, but the strongest band falls at significantly lower energy than either the strongest band in the cation or anion of APA.

Conclusions

The neutral dibenzopolyacene molecules exhibit mid-infrared spectra that are consistent with other PAHs except for having a much stronger band at about 1440 cm^{-1}. We assign this unusual band to an in-plane C–H bending mode. In the CH out-of-plane bending region we find a coupling of the trio and quartet hydrogens, while in the C–H stretching region, we find a coupling of the solo and trio hydrogens at the bay sites. The agreement between theory and experiment of approximately 10–15 cm^{-1} for all of the neutral species is consistent with previously studied PAH molecules. The B3LYP and BP86 functionals are in good agreement as expected.

The spectra of the larger dibenzopolyacene ions are much more complex than those of previously studied PAHs due to the strong electronic transitions that fall in the mid-IR overlapping with and complicating the analysis of the vibrational transitions. In the worst case, for NPN^-, many of the vibrational bands are obscured by the electronic transitions. These low-lying excited states also result in the failure of the B3LYP functional. For NPB^+ the problem is so severe that even the BP86 functional fails. In spite of these complications, in general, we find reasonable agreement between theory and experiment for the vibrational band positions. Despite the atypical mid-IR ion spectra in dibenzopolyacenes, the polyacenes and dibenzopolyacenes exhibit NIR spectra that are surprisingly consistent, showing a strong feature at around 1 μm. The unique electronic properties of the dibenzopolyacenes combined with their stability relative to their parent polyacenes warrants further investigation, especially for materials science applications.

Acknowledgments

A.R. thanks the NASA's Astrophysics Data Analysis Program (ADAP) (NN11AG11G) for their generous support of this work. We would like to thank the NASA Astrophysics Research and Analysis Program (ARA) (10-APRA10-0167) for their generous support of this research.

Appendix A. Supplementary data

Supplementary data associated with this article can be found, in the online version, at http://dx.doi.org/10.1016/j.saa.2014.04.017.

References

[1] C.A. Menzie, B.B. Potocki, J. Santodanto, Environ. Sci. Technol. 26 (1992) 1278.
[2] N.J. Aquilina, J.M. Delgado-Saborit, C. Meddings, S. Baker, R.M. Harrison, P. Jacob III, M. Wilson, L. Yu, M. Duan, N.L. Benowitz, Environ Int. 36 (2010) 763.
[3] B.J. Mahler, P.C. Van Metre, J.L. Crane, A.W. Watts, M. Scoggins, E.S. Williams, Environ. Sci. Technol. 46 (2012) 3039.
[4] C. Lambert, Angew. Chem. Int. Ed. 50 (2011) 1756.
[5] T. Chen, R. Liu, Org. Lett. 13 (2011) 4644.
[6] J. Wu, W. Pisula, K. Müllen, Chem. Rev. 107 (2007) 718.
[7] A. Li, B.T. Draine, Astrophys. J. Lett. 760 (2012) L35.
[8] C.W. Bauschlicher Jr., C. Boersma, A. Ricca, A.L. Mattioda, J. Cami, E. Peeters, F. Sanchez de Armas, G.P. Saborido, D.M. Hudgins, L.J. Allamandola, Astrophys. J. Suppl. 189 (2010) 341.
[9] E. Clar, Polycyclic Hydrocarbons, vol. 1, Academic Press, New York, 1964.
[10] J.E. Anthony, Chem. Rev. 106 (2006) 5028.
[11] W. Jiang, Y. Li, Z. Wang, Chem. Soc. Rev. 42 (2013) 6113.
[12] M.D. Watson, A. Fechtenötter, K. Müllen, Chem. Rev. 101 (2001) 1267.
[13] R. Mondal, C. Tönshoff, D. Khon, D.C. Neckers, H.F. Bettinger, J. Am.Chem. Soc. 131 (2009) 14281.
[14] E. Clar, Chem. Ber 10 (1942) 511.
[15] H.F. Bettinger, R. Mondal, D.C. Neckers, Chem. Commun. (2007) 5209.
[16] C. Tönshoff, H.F. Bettinger, Angew. Chem. Int. Ed. 49 (2010) 4125.
[17] M.M. Payne, S.R. Parkin, J.E. Anthony, J. Am. Chem. Soc. 127 (2005) 8028.
[18] D. Chun, Y. Cheng, F. Wudl, Angew. Chem. Int. Ed. 47 (2008) 8380.
[19] I. Kaur, N.N. Stein, R.P. Kopreski, G.P. Miller, J. Am. Chem. Soc. 131 (2009) 3423.
[20] J.L. Weisman, A.L. Mattioda, T.J. Lee, D.M. Hudgins, L.J. Allamandola, C.W. Bauschlicher, M. Head-Gordon, Phys. Chem. Chem. Phys. 7 (2005) 109.
[21] A.L. Mattioda, D.M. Hudgins, L.J. Allamandola, Astrophy. J. 629 (2005) 1188.
[22] A.L. Mattioda, L. Rutter, J. Parkhill, M. Head-Gordon, T.J. Lee, L.J. Allamandola, Astrophys. J. 680 (2008) 1243.
[23] D.M. Hudgins, L.J. Allamandola, Astrophys. J. Lett. 513 (1999) L69.
[24] D.M. Hudgins, S. Sandford, J. Phys. Chem. A 102 (1998) 329.
[25] H.G. Kjaergaard, T.W. Robinson, K.A. Brooking, J. Phys. Chem. A 104 (2000) 11297.
[26] A. Ricca, C.W. Bauschlicher, C. Boersma, A.G.G.M. Tielens, L.J. Allamandola, Astrophys. J. 754 (2012) 75.
[27] M.J. Frisch, J.A. Pople, J.S. Binkley, J. Chem. Phys. 80 (1984) 3265 (and references therein).
[28] C.W. Bauschlicher, S.R. Langhoff, Spectrochim. Acta A 53 (1997) 1225.
[29] A.D. Becke, J. Chem. Phys. 98 (1993) 5648.
[30] P.J. Stephens, F.J. Devlin, C.F. Chabalowski, M.J. Frisch, J. Phys. Chem. 98 (1994) 11623.
[31] A.D. Becke, Phys. Rev. A 38 (1988) 3098–3100.
[32] J.P. Perdew, Phys. Rev. B 33 (1986) 8822–8824.
[33] C.D. Sherrill, M.S. Lee, M. Head-Gordon, Chem. Phys. Lett. 302 (1999) 425.
[34] C.W. Bauschlicher, A. Ricca, Mol. Phys. 108 (2010) 2647.
[35] C.W. Bauschlicher, D.M. Hudgins, L.J. Allamandola, Theor. Chem. Acc. 103 (1999) 154.
[36] C. Boersma, C.W. Bauschlicher, L.J. Allamandola, A. Ricca, E. Peeters, A.G.G.M. Tielens, Astron. Astrophys 511 (2010) A32.
[37] Frisch MJ et al., Gaussian 09, Revision C.01, Gaussian, Inc., Wallingford CT, 2010.
[38] P. Flükiger, H.P. Lüthi, S. Portmann, J. Weber, MOLEKEL 4.2; Swiss Center for Scientific Computing: Manno, Switzerland, 2000.
[39] D.M. Hudgins, L.J. Allamandola, J. Phys. Chem. 99 (1995) 3033.
[40] D.M. Hudgins, L.J. Allamandola, Astrophys. J. Lett. 516 (1999) L41.
[41] C.W. Bauschlicher, E. Peeters, L.J. Allamandola, Astrophys. J. 697 (2009) 311.
[42] C. Lee, W. Yang, R.G. Parr, Phys. Rev. B 37 (1988) 785–789.
[43] A.L. Mattioda, D.M. Hudgins, C.W. Bauschlicher, M. Rosi, L.J. Allamandola, J. Phys. Chem. A 107 (2003) 1486.